RSC Advances

ROYAL SOCIETY OF CHEMISTRY

www.rsc.org/advances

PAPER

Occurrence of non-equilibrium orthorhombic SnO_2 phase and its effect in preferentially grown SnO_2 nanowires for CO detection

Manjeet Kumar[a], Akshay Kumar[b] and A. C. Abhyankar*[a]

Tin oxide nanowires (NWs) have been successfully deposited on the silicon substrates by the thermal evaporation of tin powder and used for gas sensing applications. This method has a good potential for large-scale fabrication of one dimensional (1D) metal oxide materials. Deposited NWs have been characterized by XRD and FESEM. XRD analysis revealed that SnO_2 NWs exhibit mixture of
10 orthorhombic and tetragonal phases or single phase tetragonal structure depending on source to substrate distance besides, it also plays a vital role on the size and morphology of NWs. The effect of multiphase SnO_2 NWs on CO sensing is studied using indigenously built sensing setup. The FESEM micrographs reveal that tin oxide NWs of about 50 to 350 nm in diameter can be grown by suitable process parameters like partial O2 pressure and distance between the substrate and source. CO sensitivity measurements
15 exhibit enhancement in case of mixed phase SnO_2 NWs as compared to single phase NWs. Texture coefficient is found to have profound effect on sensing properties of SnO_2-NWs.

1. INTRODUCTION

Among various semiconductors SnO_2 is the most attractive
20 multifunctional material being used in transparent conducting glass [1], lithium ion rechargeable batteries [2], energy storages [3], piezoelectricity [4], field emission displays [5], heterogeneous oxidation catalyst [6], photoluminescence [7] and gas sensors [8] etc. It is also a biodegradable and biocompatible
25 material, suitable for medical and biological applications [9]. As compared to other II-VI group compound semiconductors, SnO_2 has direct and wide-band gap ($E_g = 3.6$ eV at room temperature) and high exciton binding energy of 130 meV, which makes the exciton state stable even at room temperature. Band gap
30 tailoring can be done using nanostructures of SnO_2 by a variety synthesis techniques namely R-F magnetron sputtering [10], chemical vapor deposition (MOCVD) [11], spray pyrolysis [12], sol gel [13], hydrothermal

35

[a] Department of Materials Engineering, DIAT (DU), Girinagar, Pune, Maharashtra, Ministry of Defence, Email: ashutoshabhyankar@gmail.com, Fax: (020) 2438-9509, Tel
40 *(020) 2430- 4311*
[b] Department of Nanotechnology, Sri Guru Granth Sahib World University, Fatehgarh Sahib- 140406

process [14], template growth process [15] etc. Bulk SnO_2
45 sensors have tetragonal rutile (R-) phase, however, Zn doping [16] is found to stabilize high temperature and high pressure orthorhombic (O-) phase of SnO_2 along with tetragonal rutile SnO_2 when the molar ratio of Zn/Sn is around 0.133; these mixed phase thin films exhibited enhanced sensor response to
50 CO detection [16]. However, whether Zn doping alone or orthorhombic structure itself is responsible for the enhancement in sensitivity is not known. Although it is difficult to stabilize the O-phase of SnO_2 at normal atmospheric conditions, SnO_2 nanowires (NWs) synthesized on silicon substrate by thermal
55 evaporation of tin powder in controlled atmosphere exhibited mixed phases (R +T) or single rutile (R) phase depending on distance between the substrate and evaporation source. This method has a potential for large-scale fabrication of one dimensional (1D) metal oxide materials. In this paper, we
60 present XRD, FESEM and sensor measurement results on these NWs in order to clarify the effect of orthorhombic phase SnO_2 on CO detection.

2. Experimental

2.1 Synthesis

65 Fig. 1 shows the experimental set up for the deposition of SnO_2 NWs. It consists of horizontal tubular furnace and mass flow controller. Tin (Sn) powder from Sigma Aldrich (10 μm, 99% trace metals basis) was used as source materials for synthesis of

SnO$_2$ NWs. After that Sn powder was loaded in an alumina boat and placed inside the center of the heating zone of the furnace.
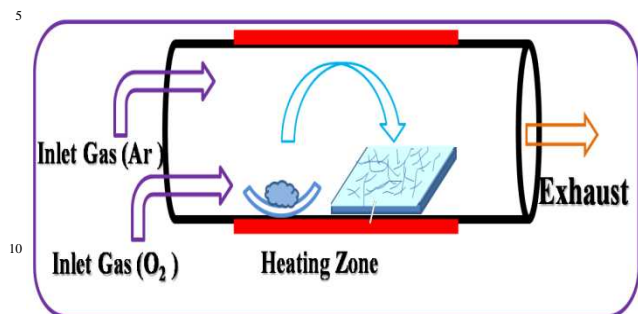
Fig. 1: Schematic sketch of Tubular furnace.

A silicon wafer with thickness: 380 ± 25µm, resistivity: 1-10 Ωcm, orientation: <100> ± 0.50 (WRS materials USA) was chosen as a substrate. These silicon substrates were placed on the downstream side at a distance of 5 cm (Sample S1) and 10 cm (Sample S2) from the source materials, and then furnace was evacuated to 10^{-2} Torr by using rotary vacuum pump and purged argon gas at 200 sccm. Then the furnace temperature was raised to growth temperature i.e. 850°C. Once the growth temperature was attained high purity oxygen gas with flow rate 50 sccm and growth process was maintained for 180 minutes. After the process flow of carrier gases were stopped and the furnace was cooled down to room temperature. These process parameters were tuned such a that sample S1 and S2 exhibited single phase tetragonal microstructure and mixed-phase (R + O) microstructure, respectively. It is found that the morphology of deposited structure depends on deposition time, substrate temperature, furnace temperature, gas flow rate however the existence of O-phase mainly depends on distance between source and substrate position. For sensing measurements, gold pattern electrodes were deposited on the on the sensing layer and the sensing area, 0.51 cm^2, was kept constant for both the sensor S1 and S2. The operating temperature was varied from 50°C to 350°C in order to find out the optimum working temperature with varying concentrations of CO gas passed to the sensing chamber using mass flow controller. Change in resistance of the sensor films was measured as a function of time through a computer interfaced EXTECH MultiMaster^{TM} 560A True RMS digital multimeter. Detailed description of indigenous sensing setup is already reported in elsewhere [17].

2.2 Characterization tools

All the samples were characterized by X-ray diffraction (XRD) using Bruker AXS, Germany (Model D8 Advanced) diffractometer in the scanning range of 20-80° (2θ) using CuKα radiation (λ=1.5418A˚). Surface morphology of these deposited nanowires was studied by Carl Zeiss Field Emission Scanning Electron Microscope (Carl Zeiss AG, Germany). The sensor testing was carried out by indigenous sensing set up.

3. Results and discussions

3.1 XRD analysis

Fig. 2 display XRD patterns of S1 and S2 samples. All the Bragg diffraction peaks of S1 can be indexed to cassiterite (R-rutile) structure of SnO$_2$ with tetragonal lattice parameters $a = b$ = 4.738(1) A˚ and c = 3.1855(9) A˚ consistent with ICDD 85-0423 whereas S2 exhibits a few but distinct peaks of orthorhombic (O-) phase (ICDD 78-1063) along with majority R-phase. The volume fraction of O-phase in S2, is estimated by calculating the ratio (I_O/I_R) of the intensity of the strongest orthorhombic reflection (111) to the intensity of the strongest tetragonal reflection (110), [18] revealed that S2 contains 8% of O-phase and 92% of R-phase. Generally orthorhombic structured SnO$_2$ is formed under high pressures at this temperature [19]. Orthorhombic phase formation at moderate temp and low pressure in oxygen deficient atmosphere has also been reported in literature [19-21].
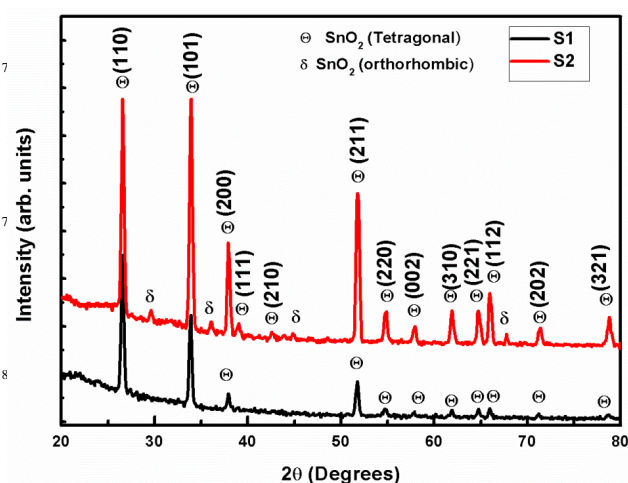
Fig. 2: XRD pattern of SnO$_2$ NWs deposited at 850°C (a) 5cm away (S1) (b) 10 cm away (S2) from the source material.

Detailed texture studies based on Harris's analysis is performed in order to calculate texture coefficient of R-phase using the relationship [22]:

$$P(h_i k_i l_i) = \frac{I(h_i k_i l_i)}{I_0(h_i k_i l_i)} \left[\frac{1}{n} \sum_{i=1}^{n} \frac{I(h_i k_i l_i)}{I_0(h_i k_i l_i)} \right]^{-1} \quad (1)$$

where P (h k l) is the texture coefficient of the plane specified by Miller Indices (h k l); I(h k l) and I$_0$(h k l) are the specimen and standard integrated intensities respectively for a given peak and n is the number of diffraction peaks. Comparison of texture coefficients of different planes (Table 1) reveals that for S1, nanowires are highly textured along (110) plane which has highest packing fraction of planar density in rutile structure, useful for sensing, as this plane is effective in electron transfer via oxygen adions, (mostly O$^-$) [23]. In S2, growth of (110) plane in R-phase SnO$_2$ may be restricted due to the presence of O-phase as evidenced by reduced texture coefficient of (110)

plane in S2 and instead strong increase in texture along (200) plane is noticed [17].

Table 1: Texture coefficient of samples S1 and S2.

Sample Name	Planes (*hkl*)	Texture coefficient
S1	110	**1.926628**
	101	1.33498
	200	**0.829961**
	211	0.474329
	112	0.434102
S2	110	**1.007898**
	101	1.112282
	200	**1.489113**
	211	0.667335
	112	0.723372

3.2 FESEM analysis

Fig. 3 shows FESEM micrographs of sample S1 and S2. NWs are clearly seen with a large aspect ratio in the range of 40-50.
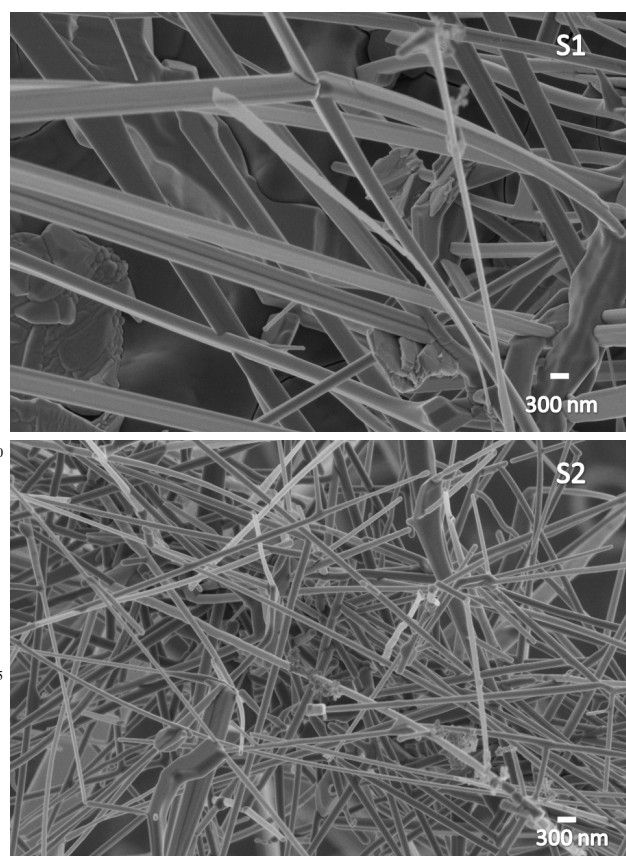
Fig.3: FESEM micrograph of S1 and S2 sensors.

The diameters of the NWs are found to be in the range of 50 to 400 nm with some branchings. The thinnest NWs of 50 nm diameter were grown in sample S2 where as the highest diameter of NWs on S1 sample was in the range of 300 to 400 nm. These observations suggest that thickness of deposited NWs decrease with the distance between the substrate and the source. The NWs in both S1 and S2 showed a very good adhesion with the substrate.

3.3 TEM analysis

TEM imaging of S2 which has mixed phases (O+T) is shown in Fig 4a. NWs are of ~ 50 nm diameter is observed. The SAD pattern of S2 shown in fig. 4(b) reveals that NWs have tetragonal structure with ring patterns observed for (110) and (211) planes. However, orthorhombic phase could not be detected owing to its low volume fraction (~8 %) determined by XRD analysis. As TEM is highly localized probe, as compared to XRD. So it was not possible to conclude the existence of orthorhombic SnO_2 phase from TEM analysis.
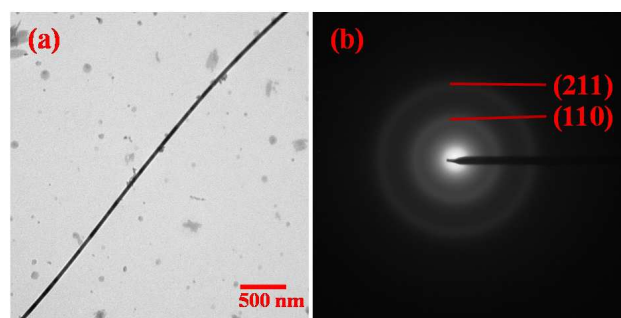
Fig.4: (a) TEM image of S2 NWs sensors, (b) Electron diffraction pattern from the nanowires shown in (a).

3.4 Sensing Measurements

Fig. 5(a, b) shows the CO sensing response of sample S1 and S2 at optimum operating temperature under the exposure of different gas concentrations. The gas sensor response is defined as:

$$S = \frac{R_a - R_g}{R_g} \times 100 \qquad (2)$$

where, R_g is the electrical resistance in presence of CO in air and R_a is the electrical resistance in air. The sensors made of NWs from S1 & S2 were tested at a temperature range from 50°C to 300°C.

S1 shows a maximum response at 225°C and S2 shows a maximum response at 175°C for different concentration of CO. Sensing response of NWs depends upon the exchange rate of gas, density of charge carriers and hence on the temperature. It is observed that for S1 sensor the sensing response is increased with temperature up to 225°C and then decreased beyond 225°C for all gas concentrations are shown in fig. 6(c) and for S2 sensor the sensing response is increased with temperature up to 175°C and decreased beyond 175°C for all gas concentrations as shown in fig. 6(d). From fig. 5(a) and 5(b) the measured response- (recovery-) times for S1 are 1-2 sec (20-55 sec) and for S2 are 1-2 sec (15-40 sec) respectively.
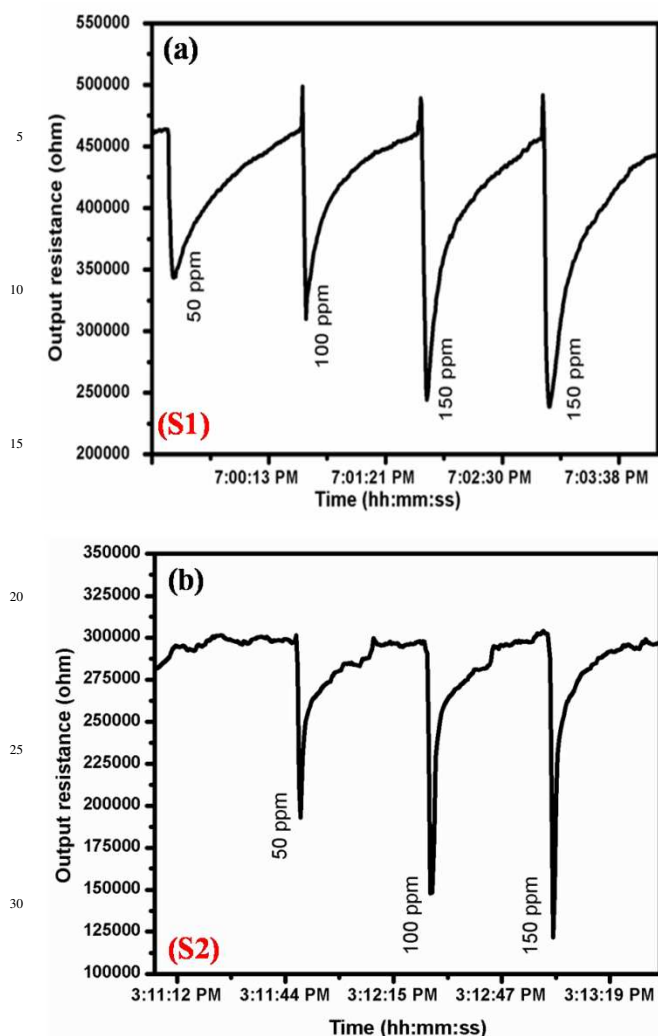
Fig. 5: Sensor response of (a) S1 for different concentration of CO at 225°C (b) S2 for different concentration of CO at 175°C as a function of time.

The sensors were capable of detecting CO in the range of 50-150 ppm at temperatures 50°C to 300°C and recover quickly once the CO is removed as shown in fig. 6 (a) & (b). S1 and S2 NW's exhibit a maximum sensitivity of 102 and 150 for 150 ppm of CO, respectively. These results show that mixed phase NWs with (R + O) structure exhibit higher sensitivity than single (R-) phase NWs. Our results also indicate that large surface area available due to reduction in diameter of NWs also plays a very important role for sensitivity of the sensors which is also supported by literature [24, 25]. These results are also consistent with texture analysis. Texture coefficients calculated for different Miller planes are tabulated in Table 1. It reveals that as compared to samples S1, the texture coefficient of (200) plane increased noticeably in S2, at the cost of decrease in planar density along (110) plane. Such a change in texture coefficients was reported earlier with dopants like Fe, In and W [17, 26]. Reduced texture coefficient of dense (110) plane can act as sink of vacancies and thereby improve sensing response in

S2.
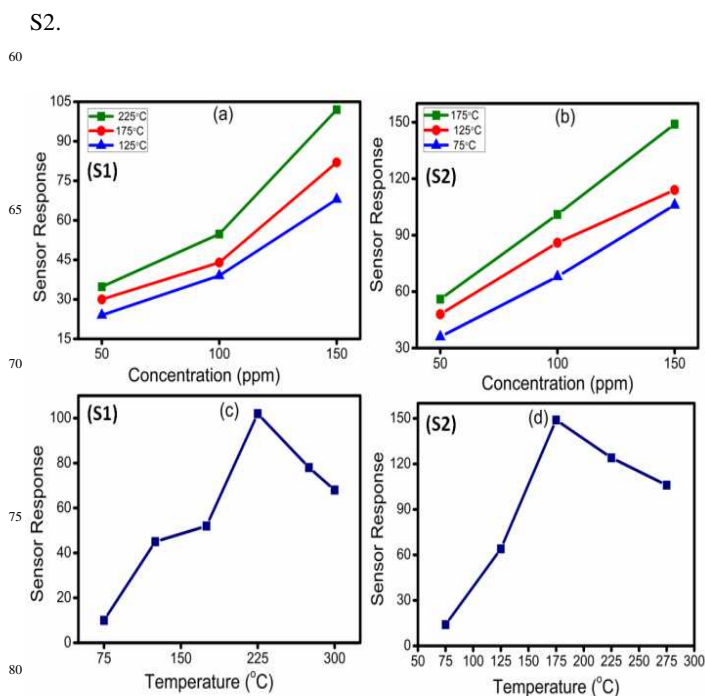
Fig. 6: Sensor response of S1 and S2 as a function of concentration (a,b) & temperature (c, d).

Cross sensitivity behavior of these sensors S1 and S2 was tested with 150 ppm of CO, C_2H_5OH and NH_3 gas are shown in fig. 7. It is confirmed from the fig. 7 that S2 sensor is highly sensitive to CO gas at its working temperature 175°C. The several literature reports revealed that pure SnO2 is selective for CO at particular operating temperature [27-29].
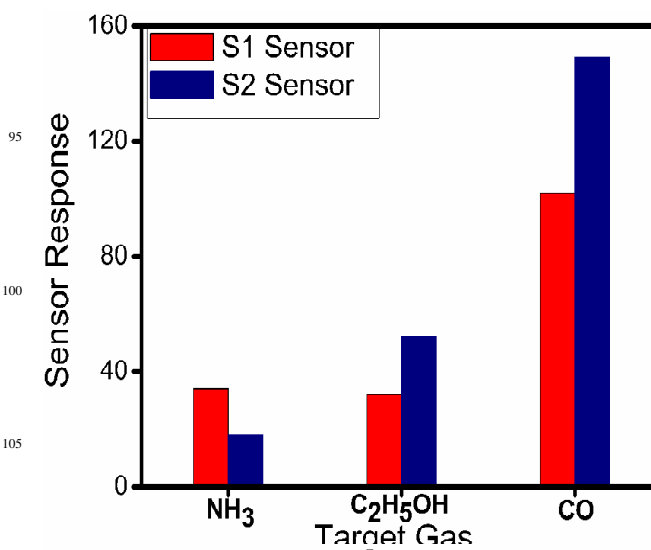
Fig.7: Sensors response of S1 and S2 sensors for different target gases at 150 ppm.

The higher sensor response of S2 sample for CO, as seen from fig.7, in the present work, might be due to NWs of smaller diameters, mixed phase and huge reduction in texture coefficient along most densely packed (110) plane.

4. Conclusions

Preferentially grown NWs along (110) and (200) plane are deposited on silicon substrate at deposition temperature 850°C. The NWs have average diameter of 50~350 nm. The XRD studies reveal that formation of tetragonal and mixed phase (orthorhombic and tetragonal) SnO_2 NWs and electron microscopy studies reveal the formation of tin oxide NWs. It is found that the texture coefficient and diameter of NWs plays a very important role for sensitivity of the sensors. It clearly indicates that sensor response decreases with increasing texture coefficient along (110) plane and increases with increasing texture coefficient of (200) concurrent reduction in texture coefficient of most dense (200) plane. The mixed orthorhombic and rutile phase SnO_2 NWs with diameter (50-200 nm) exhibit enhanced sensitivity for CO detection as compared to single phase.

Acknowledgements

REFERENCES

[1] N. Kikuchi, E Kusano, E Kishio, A Kinbara, *Vacuum,* 2002, **6** 365-371.

[2] Yaomin Zhao, Qin Zhou, Ling Liu, Juan Xu, Manming Yan, Zhiyu Jiang, *Electrochimica Acta,* 2006, **51**, 2639.

[3] Jun Seop Lee, Jyongsik Jang, *Journal of Industrial and Engineering Chemistry,* 2014, **20**, 363-371.

[4] Shi Su, Ruzhong Zuo, Xiaohui Wang, Longtu Li., *Materials Research Bulletin,* 2010, **45** 124-128.

[5] Ziqiang Zhu., *Applied Surface Science,* 2006, 253, 792-796.

[6] Sarah Pilkenton, Daniel Raftery., *Solid State Nuclear Magnetic Resonance,* 2003, **24**, 236-253.

[7] Li-Wei Chang, Meng-Wen Huang, Chung-Tien Li, Han C. Shih., *Applied Surface Science,* 2013, **279,** 167-170.

[8] Matthias Batzill, Ulrike Diebold., *Progress in Surface Science,* 2005, **79**, 47–154.

[9] L.Wang, Y. Chen, J. Ma, L. Chen, Z. Xu, T. Wang, *Sci. Rep.* 3, 3500; DOI:10.1038/srep03500 (2013).

[10] Wenhao Yang, Shihui Yu, Yang Zhang, Weifeng Zhang., *Thin Solid Films,* 2013, **542**, 285-288.

[11] R.Y. Korotkov, P. Ricou, A.J.E. Farran., *Thin Solid Films,* 2006, **502**, 79-87.

[12] G. Korotcenkov, I. Blinov, M. Ivanov, J.R. Stetter, *Sensors and Actuators B: Chemical,* 2007, **120**, 679-686.

[13] Xiaohua Zhong, Baoping Yang, Xiaoliang Zhang, Junhong Jia, Gewen Yi, *Particuology,* 2012, **10**, 365-370.

[14] Yue Guan, Dawei Wang, Xin Zhou, Peng Sun, Haiyu Wang, Jian Ma, Geyu Lu., *Sensors and Actuators B Chemical,* 2014, **191**, 45-52.

[15] Chunlong Zheng, Xiangzhen Zheng, Zhensheng Hong, Xiaokun Ding, Mingdeng Wei., *Mater Lett*., 2011, **65**, 1645-1647.

[16] S Tian, Yingri Gao, Dawen Zeng, and Changsheng Xie, *J. Am. Ceram. Soc.,* 2012, **95**, 436–442.

[17] M. Kumar, A. Kumar, A.C. Abhyankar., *Ceram. Int*., 2014, **40**, 8411–8418.

[18] R. A. Spurr and H. Myers, *Anal. Chem.,* 1957, **29,** 760.

[19] F. J. Lamelas, S. A Reid, *Physical Review B* 1999, **60** 9347- 9352

[20] Z. R. Dai, Z. Wei Pan, Z. L. Wang, *Adv. Funct. Mater.* 2003, **13,** 9-24

[21] Z. R. Dai, J. L. Gole, J. D. Stout, Z. L. Wang, *J. Phys. Chem. B* 2002, **106** 1274-1279

[22] G.B. Harris., *Philos. Mag.,* 1952, **43**, 113.

[23] M.A. Maki-Jaskari, T.T. Rantala, *Physical Review B,* 2002, **65,** 1–6.

[24] D. Meng, N. M. Shaalan, T. Yamazaki, T. Kikuta, *Sensors and Actuators B* 2012, **169** 113-120

[25] N. M. Shaalan, T. Yamazaki, T. Kikuta, *Sensors and Actuators B* 2011, **153** 11-16

[26] M. Kumar, A. Kumar, A. C. Abhyankar, *ACS Appl. Mater. Interfaces* 2015, **7** 3571-3580

[27] G. Tulzer, S. Baumgartner, E. Brunet, G. C. Mutinati, S. Steinhauer, A. Kock, C. Heitzinger, *SciVerse ScienceDirect* 2012, **47** 809-812

[28] A. M. Gaskov, M. N. Rumyantseva, Inorganic Materials, 2000, **36** 293-301

[29] P. G. Harrison, M. J. Willet, *Nature* 1998, **332** 337-339

Graphical Abstract

Inlet Gas (Ar)

Inlet Gas (O_2)

Exhaust

Gold Contacts